Citation

Haq, M. Z. (March 16, 2021). "Optimization of an Organic Rankine Cycle-Based Waste Heat Recovery System Using a Novel Target-Temperature-Line Approach." ASME. J. Energy Resour. Technol. September 2021; 143(9): 092101.
https://doi.org/10.1115/1.4050261

Optimization of organic Rankine cycle (ORC) based waste heat recovery (WHR) system using a novel target-temperature-line approach

Md. Zahurul Haq
Professor, Department of Mechanical Engineering,
Bangladesh University of Engineering and Technology (BUET), Dhaka-1000, Bangladesh
Email: zahurul@me.buet.ac.bd, Z.Haq95@members.leeds.ac.uk
www: http://zahurul.buet.ac.bd/

ABSTRACT

Organic Rankine cycle (ORC) based waste heat recovery (WHR) systems are simple, flexible, economical and environment-friendly. Many working fluids and cycle configurations are available for WHR systems, and the diversity of working-fluid properties complicates the synergistic integration of the efficient heat exchange in the evaporator and net output work. Unique guidelines to select proper working-fluid, cycle configuration and optimum operating parameters are not readily available. In the present study, a simple target-temperature-line approach is introduced to get the optimum operating parameters for the sub-critical ORC system. The target-line is the locus of temperatures satisfying the pinch-point-temperature-difference along the length of the heat-exchanger. Employing the approach, study is carried out with 38 pre-selected working fluids to get the optimum operating parameters and suitable fluid for heat source temperatures ranging from 100°C to 300°C. Results obtained are analysed to get cross-correlations between key operating and performance parameters using heat-map diagram. At the optimum condition, optimal working fluid's critical temperature and pressure, evaporator saturation temperature, effectivenesses of the heat exchange in the evaporator, cycle and overall WHR system exhibit strong linear correlations with the heat source temperature.

Keywords: Organic Rankine cycle (ORC), Waste heat recovery (WHR), Energy efficiency, Pinch point, Thermodynamic optimization.

Nomenclature

D heat exchanger duty (J)

h, H enthalpy (J/kg, J)

I irreversibility (J)

P pressure (Pa)

r (Pearson's) correlation coefficient

T temperature (^{o}C)

W work (J)

Greek Letters

ε (second-law) effectiveness

η first-law efficiency

Ψ, ψ flow-exergy (J, J/kg)

Superscripts and Subscripts

. (e.g. $\dot{m}$, $\dot{W}$) rate of (e.g. mass flow, work)

0 environmental state

01–06 thermodynamic state points

c cold fluid stream

cr critical-point state

cy cycle

evap evaporator

h hot fluid stream

ht heat transfer

in inlet

net net

o overall

out outlet

p pump

pp pinch point

sat saturated condition

t turbine

wf working fluid

Acronyms

ORC organic Rankine cycle

WHR waste heat recovery

1 Introduction

With the increasing uncertainty in the supply and price of fuels, and the global warming challenges because of greenhouse gas (GHG) emissions, efficient energy conversion is vital to simultaneously address energy security and environmental issues. During conversion to useful work, around half of the primary energy is lost as 'waste heat' and 40% of the lost heat is in the temperature ranging from 80°C to 300°C [1]. Hence, 'waste heat' is defined as 'waste heat as a resource is exergy that unavoidably leaves a process or is lost within it independent of the technological choices made within the process' [2]. Effective utilization of waste heat boosts overall system performance with simultaneous reduction in primary energy consumption and carbon footprint [3]. Among the technologies to convert the medium-to-low grade thermal energy into power, waste heat recovery (WHR) systems based on organic Rankine cycle (ORC) offer the advantages of flexibility, efficiency, simplicity, safety and stability [4]. Turbines built for ORC systems typically require single stage-expander, resulting in a simple and economical system in terms of capital costs and maintenance [5].

Recently, research and applications of ORC based WHR systems are expanding globally. These are implemented to economically utilize waste heat from engines (e.g. automotive- [6], Diesel- [7] and gas- [8] engines), industrial processes (e.g. cement [9], steel [10], smelting furnace gases [11], boiler flue gas [12], etc.) and renewable energy sources like geothermal [13, 14], solar thermal [15], biomass [16], etc. The availability of various working fluids [5, 17], optimized components [18, 19] and design alternatives for cycle/configuration [13, 20] enable the ORC systems to economically operate in a wide range of heat source temperatures and capacities.

In the WHR system, hot source fluid forms an external coupling with the evaporator of the ORC. The variation in the heat capacity rates of the heat source fluid is small and therefore exhibit essentially linear heat-release-curve. However, thermophysical properties of the working fluids differ remarkably in preheating, evaporation and super-heating, and typical heat absorption curve is a poly-line in the T-S diagram [4]. So, local heat capacity rates of the heat exchanging fluids are not well-matched in the evaporator and the unavoidable temperature difference leads to the major contribution to overall exergy destruction [21].

For a heat source, several thermophysical properties are to be weighted to select proper working fluid: molecular-structure and complexity, fluid's critical properties, normal boiling point and evaporation pressure, latent heat of evaporation, liquid and two-phase heat capacities and the slope of the fluid vapour saturation line in T-S diagram, etc. [20]. Addressing all these parameters is tedious, and fluid's critical temperature is the commonly used parameter for the selection of potential working fluids [20]. The slope of the expansion process of the working fluid in a T-S diagram is also important: the slope can be positive, negative or vertical and the fluids are accordingly termed as 'dry', 'wet' and 'isentropic', respectively [22]. Isentropic and dry fluids are widely used in the ORC systems as wet fluids need to be superheated to minimize turbine blade 'pitting' caused by fluid droplets during expansion. However, if the fluid is too dry, the expanded fluid leaves with substantial superheat causing energy loss [5]. Recently, some fluids are fruitfully classified as 'super dry' [23].

To recover waste heat, several cycle configuration/options are available [1, 20]. A trans-critical cycle can increase the efficiency; however, with lower heat absorption capacity and the adaptability to different heat sources [4]. Dual-pressure evaporation may significantly increase the heat absorption capacity with improved adaptability to heat sources, while the temperature difference between the fluids remains large for high-temperature heat sources [4]. Dual-loop systems achieve the maximum power output; however, these are large, complex and often economically unfavourable, particularly for the automotive applications [6]. Updated version of a single-loop system can overcome some of the limitations [6]. At a source temperature, optimized single-loop ORC system with a pure working fluid can provide important guidance to design mixture

working fluid for proper thermal matching for high heat exchange efficiency [24].

For maximum heat recovery, 'pinch point' analysis is vital [25]. Costs of the WHR systems decrease with an increase in pinch point temperature difference, ΔT_{pp}, while the exergy destruction in the evaporator is increased [26]. With every 1°C decrease in evaporator ΔT_{pp}, ORC systems produce 1.7 - 2.6% more net work output [27]. Hence, proper selection of ΔT_{pp} is vital to optimize efficiency and capital investment, as heat-exchangers (evaporator and condenser) account for the largest portion of the required investment [23]. The optimal value of ΔT_{pp} are reported in the range of 5-12°C [21], and 7-10°C [28]; and, ΔT_{pp} = 10°C is widely used [29]. Several alternative approaches are employed to implement pinch in the heat-exchanger design: pinch and exergy are integrated into heat exchanger network (HEN) [30, 31]; suitable algorithm is applied to predict pinch point locations in the heat-exchanger and then optimization is sought [32]; by defining parameters to address preheating and vaporizing pinch points followed by the optimization of the operating parameters [33], using a framework enabling the simultaneous optimization of the processes [34]. Recently, Rad et al. [29] proposed some simultaneous optimization of the working fluid and the operating parameters; however, evinced the non-availability of a unique procedure to achieve maximum utilization of the waste heat.

Experimental works form a small fraction of the published literature in the ORC-technology and experimentations are often carried out for various heat source fluids (e.g. hot exhaust gases, water, oil etc.) at various temperatures and are subjected to various environmental states. Most of the experimental ORC-systems are constructed with basic ORC configurations predominantly for low-medium temperature heat sources because of the huge potential of the industrial applications, and R245fa is found to be the most popular working fluid [35]. Feng et al. [36] reported the experimental comparison of the performance of the basic and regenerative ORC systems using R245fa as the working fluid, and observed the lower temperature utilization of the regenerative ORC systems than the basic ORC systems as the addition of the regenerator leads to the heating of the working fluid entering the evaporator resulting in reduced heat absorbency. Moreover, the addition of the recuperator/regenerator increases in the capital cost and the space requirement to put some limitations for some applications, especially for low-medium temperature heat sources. Recently, based on the survey of more than 200 experimental ORC systems, the maximum output of the systems are found around 7% lower than the target power or the nominal power of the expander requiring to oversize the systems by at least 7% further [35].

In the present study, a simple approach using a target-temperature-line is proposed and demonstrated to select optimal working fluid and optimum operating parameters for the sub-critical ORC system to maximize the waste heat utilization. The proposed method decouples the heat exchange process from the power cycle, and provides a range of feasible operating parameters satisfying the design constraints for the heat exchangers. The approach is simple to implement and applicable for pure working fluids and fluid-mixtures. The feasible operating parameters are then used for the detailed optimization of the power cycle. In the present paper, study is reported for heat sources at 9 different temperatures ranging from 100 to 300°C, and key operating and performance parameters are obtained for the sub-critical ORC based WHR systems. At the optimum condition(s) with optimal working fluid(s), optimal fluid's critical temperature and pressure, the cycle's evaporator saturation temperature and some key performance parameters are found to exhibit strong linear correlations with the heat source temperatures.

2 Methodology

2.1 Thermodynamic Model

Waste heat recovery (WHR) system, considered in the present study, is based on the organic Rankine cycle (ORC) which is composed of four key components as shown in Fig. 1, and the thermodynamic state-points are designated by two-digit numbers. Hence, heat source fluid forms an external coupling with the evaporator of the ORC system and three physical/virtual regions could be identified in the evaporator: 'H-01' is the pre-heater/economiser, evaporation occurs at 'H-02' and 'H-03' is the super-heater; and superheating of the working fluid may not occur and evaporation then continues in the last two regions. Working fluid vapour, generated in the evaporator, is expanded in the turbine (expander) to produce useful work. Vapour leaving the turbine is then condensed to saturated state and pumped back to the evaporator for the cycle completion. In the present study, steady-state-steady-flow (SSSF) operation and negligible pressure drops in the evaporator, condenser and the piping system are assumed. In general, variation in the heat capacity rates of heat source fluid (e.g. exhaust gases, waste hot water etc.) is small and dry-air is assumed as the heat source fluid in the present study to demonstrate the proposed methodology which can be applied even if the heat exchanging fluids exhibit variable heat capacity or even phase change(s). When exhaust gases are used as the heat source, chimney draught requirement and the dew-point temperature of the gas impose some limitations of the final outlet temperature. Rad et al. [29], used 60°C as the final exit temperature assuming the absence of sulphur in the exhaust gases. In the present study, evaporator outlet temperature is assumed to be 60°C to assess the maximum feasible heat recovery from the waste heat source. Some base-operating-parameters of the present study are reported in Table 1.

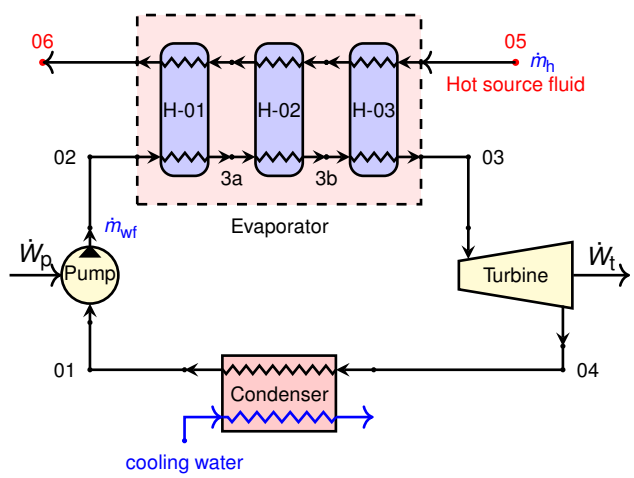

Fig. 1: Schematic block diagram of the system.

If energy balance is performed on each of the system components, the 'SSSF energy equation', neglecting the change in potential and kinetic energy, can be written, in general, as [38]:

$$\dot{Q} = \dot{W} + \sum_{i}^{out} \dot{m}_i h_i - \sum_{i}^{in} \dot{m}_i h_i \tag{1}$$

where $\dot{Q}$ is the heat transfer rate into the component, $\dot{m}_i$ is the working fluid's mass flow rate at section 'i', h_i is the enthalpy at section 'i' and $\dot{W}$ is the work rate by the component. Similarly, the 'SSSF exergy equation' can be expressed as [38]:

$$\dot{\Phi}_Q = \dot{W} + \sum_{i}^{out} \dot{m}_i \psi_i - \sum_{i}^{in} \dot{m}_i \psi_i + \dot{I} \tag{2}$$

Table 1: Base-operating-parameters of the WHR system.

Parameter	Symbol	Value
Hot Source		
Fluid [37]		Dry air
Mass flow rate	$\dot{m}_{\mathrm{h}}$	1.0 kg/s
Inlet temperature	$T_{\mathrm{h,in}}$	[100-300]^{o}C
Outlet temperature [29]	$T_{\mathrm{h,out}}$	60°C
ORC system		
Condenser pressure [29]	P_{cond}	sat. at 30°C
Evaporator saturated temperature	$T_{\mathrm{evap,sat}}$	$\leq 0.95T_{\mathrm{cr}}$
Fluid quality in/out turbine [29]	X_{03}, X_{04}	≥ 0.90
Pump isentropic efficiency [29]	η_{p}	0.70
Turbine isentropic efficiency [29]	η_{t}	0.85
Pinch-point temperature difference [29]	ΔT_{pp}	10°C
Environmental State		
Temperature	T_0	25°C
Pressure	P_0	0.1 MPa

where $\dot{\Phi}_{\mathrm{Q}} \equiv \sum Q_i \left(1 - \frac{T_0}{T_i}\right)$ is the exergy transfer associated with heat transfer, $\dot{I}$ accounts for exergy destruction because of internal irreversibility in the component and ψ_i is the flow-exergy at section 'i'. Hence, flow-exergy is defined as:

$$\psi \equiv (h - h_0) - T_0(s - s_0) \tag{3}$$

where, kinetic and potential energies are omitted, and the subscript '0' represents the properties of the fluid at (restricted) equilibrium with the environment [39] and T_0 is expressed in absolute scale.

In the evaporator, heat source fluid enters at $T_{\mathrm{h,in}}$ and leaves at $T_{\mathrm{h,out}}$, and no work is produced. Considering negligible heat exchange with the environment, simplified energy and exergy balance equations (Eqs. 1 and 2), respectively, are:

$$\dot{m}_{\mathrm{wf}}(h_{03} - h_{02}) = \dot{m}_{\mathrm{h}}(h_{05} - h_{06}) \tag{4}$$

$$\dot{m}_{\mathrm{h}}(\psi_{05} - \psi_{06}) = \dot{m}_{\mathrm{wf}}(\psi_{03} - \psi_{02}) + \dot{I}_{\mathrm{evap}} \tag{5}$$

where, $\dot{m}_{\mathrm{h}}$ and $\dot{m}_{\mathrm{wf}}$ are the mass flow rates of the source and working fluids, respectively.

In the evaporator, supplied exergy, $\Delta\dot{\Psi}_{\mathrm{h}} = \dot{m}_{\mathrm{h}}(\psi_{\mathrm{h,in}} - \psi_{\mathrm{h,out}}) = \dot{m}_{\mathrm{h}}(\psi_{05} - \psi_{06})$, is not completely transferred to the working fluid and significant exergy destruction occurs. Figure 2 shows two isobaric heat exchange processes on a typical $T - \dot{S}$ diagram, following [39], and the areas under the lines $T_{\mathrm{h,in}} - T_{\mathrm{h,out}}$ and $T_{\mathrm{c,in}} - T_{\mathrm{c,out}}$ are equal. Since $\dot{I} = T_0 \sum \Delta\dot{S}$, the shaded area represents the irreversibility, $\dot{I}_{\mathrm{evap}}$, because of heat exchange process. As the process profiles on $T - \dot{S}$ diagram approaches each other, irreversibility is reduced. In the condenser, temperature difference between the heat exchanging fluids is small and generated irreversibility is often neglected [39].

Processes in the pump and the turbine are essentially adiabatic in nature. So, using Eq. 1, the pump and turbine works can be written, respectively, as:

$$\dot{W}_{\mathrm{p}} = -\dot{m}_{\mathrm{wf}}(h_{02} - h_{01}) \tag{6}$$

$$\dot{W}_{\mathrm{t}} = \dot{m}_{\mathrm{wf}}(h_{03} - h_{04}) \tag{7}$$

Using Eq. 2, irreversibility in the pump and in the turbine can be written, respectively, as:

$$\dot{I}_{\mathrm{p}} = -\dot{W}_{\mathrm{p}} - \dot{m}_{\mathrm{wf}}(\psi_{02} - \psi_{01}) \tag{8}$$

$$\dot{I}_{\mathrm{t}} = -\dot{W}_{\mathrm{t}} - \dot{m}_{\mathrm{wf}}(\psi_{04} - \psi_{03}) \tag{9}$$

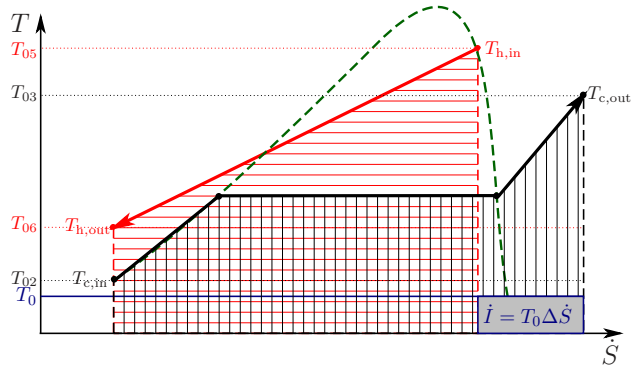

Fig. 2: Irreversibility because of heat-exchange process.

2.2 Performance Indicators

Efficiency is widely used to indicate the performance of a system. However, efficiency can have different meanings and, unaccompanied by a formal definition or taken out of context, can lead to serious misconceptions [40]. Efficiencies based on the first-law of thermodynamics fall into two general categories [39]:

1. *'Thermal efficiency'*, which compares the desired energy output to the required energy input [38, 39], that is,

$$\eta_{\mathrm{th}} \equiv \frac{\text{Energy out in product}}{\text{Energy in}} = \frac{\text{Energy out in product}}{\text{Energy out in product} + \text{Energy loss}} \tag{10}$$

   where, the term *product* may refer to shaft work or generated electricity, some desired combination of heat and work etc., and *losses* include such things as waste heat or stack gases vented to surroundings without use [38].

2. Equipment first-law efficiency, widely known as *'first-law efficiency'* or *'isentropic efficiency'*, and it compares the actual energy change to some theoretical energy change under specified condition. Many work producing/absorbing devices operate approximately adiabatic, and the comparison is often made with isentropic condition with the same initial state and the final pressure [39]. Accordingly, isentropic efficiency of the turbine and the pump can be written, respectively, as:

$$\eta_{\mathrm{t}} \equiv \frac{\dot{W}_{\mathrm{t}}}{\dot{W}_{\mathrm{t,s}}} = \frac{h_{03} - h_{04}}{h_{03} - h_{\mathrm{s},04}} \tag{11}$$

$$\eta_{\mathrm{p}} \equiv \frac{\dot{W}_{\mathrm{p,s}}}{\dot{W}_{\mathrm{p}}} = \frac{h_{\mathrm{s},02} - h_{01}}{h_{02} - h_{01}} \tag{12}$$

   where $h_{\mathrm{s},04}$ is the fluid enthalpy for isentropic expansion in the turbine and $h_{\mathrm{s},02}$ is the fluid enthalpy for isentropic compression in the pump.

Efficiency parameters based on first-law of thermodynamics make no distinction between work, heat and other forms of energy. To address the potential of heat to produce useful work, performance based on exergy concept is known as a *'second-law'* or *'exergetic efficiency'*, η_{II}, or as *'second-law effectiveness'*, or simply as an *'effectiveness'*, ε. Typical definition of second-law effectiveness, ε is [38, 40]:

$$\varepsilon \equiv \frac{\text{Exergy out in product}}{\text{Exergy in}} \tag{13}$$

Hence, the effectiveness of the WHR system is the net work output divided by the exergy input associated with the heat source; that is,

$$\varepsilon_{\mathrm{o}} \equiv \frac{\dot{W}_{\mathrm{net}}}{\dot{\Psi}_{\mathrm{h,in}}} = \frac{\dot{W}_{\mathrm{net}}}{\dot{m}_h \psi_{\mathrm{h,in}}} = \frac{\dot{W}_{\mathrm{net}}}{\dot{m}_h \psi_{05}} \tag{14}$$

Table 2: Pre-selected working fluids.

w. fluid	T_{cr} [^{o}C]	P_{cr} [MPa]	type [23]	w. fluid	T_{cr} [^{o}C]	P_{cr} [MPa]	type [23]	w. fluid	T_{cr} [^{o}C]	P_{cr} [MPa]	type [23]
R1216	85.75	3.1495	Isen.	R245fa	153.86	3.651	Dry	heptane	267.05	2.7357	S. Dry
R1234yf	94.7	3.3822	Isen.	R1233zd(E)	166.45	3.6237	Isen.	isooctane	270.85	2.572	S. Dry
R227ea	101.75	2.925	Dry	R245ca	174.42	3.9407	Dry	cyclohexane	280.45	4.0805	Dry
R1234ze(E)	109.36	3.6349	Isen.	R123	183.68	3.6618	Isen.	benzene	288.87	4.9073	S. Dry
perfluorobutane	113.18	2.3224	Dry	R365mfc	186.85	3.266	Dry	octane	295.59	2.4836	S. Dry
RC318	115.23	2.7775	Dry	isopentane	187.2	3.378	S. Dry	D4	313.35	1.3472	S. Dry
R124	122.28	3.6243	Isen.	R141b	204.35	4.212	Isen.	toluene	318.6	4.1263	S. Dry
R236fa	124.92	3.2	Dry	R113	214.06	3.3922	Dry	nonane	321.4	2.281	S. Dry
isobutane	134.66	3.629	Dry	isohexane	224.55	3.04	S. Dry	p-Xylene	343.02	3.5315	S. Dry
R236ea	139.29	3.42	Dry	pentane	232.85	3.1845	S. Dry	m-Xylene	343.74	3.5346	S. Dry
isobutene	144.94	4.0098	Isen.	hexane	234.67	3.0441	S. Dry	ethylbenzene	343.97	3.6224	S. Dry
butene	146.14	4.0051	Dry	cyclopentane	238.57	4.5828	Dry	decane	344.55	2.103	S. Dry
butane	151.98	3.796	Dry	MM	245.55	1.9311	S. Dry				

Heat-exchange effectiveness in the evaporator, ε_{ht}, is the exergy gain of the working fluid divided by the decrease of the exergy of the heat source fluid, that is,

$$\varepsilon_{ht} = \frac{\Delta\dot{\Psi}_c}{-\Delta\dot{\Psi}_h} = \frac{\dot{m}_{wf}(\psi_{03} - \psi_{02})}{\dot{m}_h(\psi_{05} - \psi_{06})} \tag{15}$$

and, effectiveness of the ORC, ε_{cy}, can be expressed as:

$$\varepsilon_{cy} = \frac{\dot{W}_{net}}{\dot{\Psi}_{cy,in}} = \frac{\dot{W}_{net}}{\dot{m}_{wf}(\psi_{03} - \psi_{02})} \tag{16}$$

So, several performance indicators are available for the WHR systems; however, waste heat recovery and output power are not generally maximized at peak thermal efficiency [1]. Recently, exergy is opined as 'the only rational basis' to assign monetary values and environmental impacts to energy conversion processes and associated thermodynamic inefficiencies within it [41]. Exergy losses indicate the scope of thermodynamic improvement, and therefore exergy based performance indicator, embedded in the concept of effectiveness, is used in the present study to identify the optimum performance of the system.

2.3 Preliminary Selection of Working Fluids

Critical temperature and type of the working fluid are widely used to pre-select the fluid. For a given heat source temperature, $T_{h,in}$, J. Hærvig et al. [37] reported that the optimal fluid has a critical temperature within 30°C to 50°C below $T_{h,in}$; however, Rad et al. [29] considered all the fluids with critical temperatures in the range of $\pm$ 40°C of $T_{h,in}$. In the present study, fluids having critical temperatures within $\pm$ 50°C of $T_{h,in}$ are considered in the fluid pre-selection and 'wet' fluids are excluded. Hence, total 38 fluids are considered and are listed in Table 2, and temperature-wise list is reported in Table 3.

2.4 Estimation of Thermophysical Properties

Thermophysical properties of the working fluids are estimated using REFPROP ver. 10 [42], which is developed by the National Institute of Standards and Technology (NIST) for the calculations of thermodynamic and transport properties of important pure and mixtures fluids. Present thermodynamic model is implemented in Python programming language, and COOLPROP [43] utilities are used to access the REFPROP library and to validate some property data. To validate, data and

Table 3: Temperature-wise pre-selected working fluids.

Heat source gas temperature, $T_{h,in}$								
100°C	125°C	150°C	175°C	200°C	225°C	250°C	275°C	300°C
R1216	R1216[1]	R227ea	isobutane	butane	R123	R141b	pentane	heptane
R1234yf	R1234yf	R1234ze(E)	R236ea	R245fa	R365mfc	R113	hexane	isooctane
R227ea	R227ea	perfluorobutane	isobutene	R1233zd(E)	isopentane	isohexane	cyclopentane	cyclohexane
R1234ze(E)	R1234ze(E)	RC318	butene	R245ca	R141b	pentane	MM	benzene
perfluorobutane	perfluorobutane	R124	butane	R123	R113	hexane	heptane	octane
RC318	RC318	R236fa	R245fa	R365mfc	isohexane	cyclopentane	isooctane	D4
R124	R124	isobutane	R1233zd(E)	isopentane	pentane	MM	cyclohexane	toluene
R236fa	R236fa	R236ea	R245ca	R141b	hexane	heptane	benzene	nonane
isobutane	isobutane	isobutene	R123	R113	cyclopentane	isooctane	octane	p-Xylene
R236ea	R236ea	butene	R365mfc	isohexane	MM	cyclohexane	D4	m-Xylene
isobutene	isobutene	butane	isopentane	pentane	heptane	benzene	toluene	ethylbenzene
butene	butene	R245fa	R141b	hexane	isooctane	octane	nonane	decane
	butane	R1233zd(E)	R113	cyclopentane				
	R245fa	R245ca	isohexane	MM				
	R1233zd(E)	R123						
	R245ca	R365mfc						
		isopentane						

[1] Non-feasible solution, no solution is found to satisfy all the imposed conditions.

Table 4: Validation using energy and exergy accounting data of a steam power plant.

Parameter(s)		present study	Data [39]
Q_{boiler}, Q_{cond}	[kJ/kg]	3315.9, -2097.9	3314.4, -2097.5
W_t, W_p	[kJ/kg]	1238.1, -20.06	1237.0, -20.1
ψ_{boiler}, ψ_{cond}	[kJ/kg]	1510.0, -75.68	1509.5, -75.9
ψ_t, ψ_p	[kJ/kg]	-1449.0, 14.28	-1447.9, 14.3
I_t, I_p	[kJ/kg]	210.6, 5.78	210.9, 5.8

results reported in the literature are checked (e.g. [39], [43]), and one particular case is presented in Table 4 where energy and exergy accounting of a Rankine cycle is compared. Good agreements are observed between the obtained results and reported in [39].

2.5 Estimation of Optimum Operating Parameters using the Target-temperature line

In the present study, a 'target-temperature line' approach is introduced to estimate the optimum operating parameters. Neglecting the heat losses to the environment, heat delivered to working fluid is known as 'Duty' of the heat exchanger [44], and its value can be estimated using:

$$D = -\Delta H_h = \dot{m}_h (h_{05} - h_{06}) \tag{17}$$

To construct the 'target-temperature line', D is equally divided into 1000 parts along the length of the heat exchanger, and at an intermediate duty D_j, the corresponding heat source fluid temperature, $T_{h,j}$, is estimated from the calculated value of $h_{h,j}$ using the heat balance equation:

$$D_j = \frac{j}{1000} D = \dot{m}_h (h_{h,j} - h_{06}) \tag{18}$$

here, h_{06} is the enthalpy of the heat source fluid leaving the evaporator. The target temperature, $T_{r,j}$, is estimated using:

$$T_{r,j} = T_{h,j} - \Delta T_{pp} \tag{19}$$

where ΔT_{pp} is pinch point temperatures difference. The target-temperature line construction is illustrated in Fig. 3. At a given D_j, the working fluid is assumed saturated at $T_{\text{r},j}$; so, $T_{\text{evap,sat},j} = T_{\text{r},j}$ and $P_{\text{evap},j}$ is the corresponding saturation pressure. Hence, D_j is consumed to preheat the working fluid to the saturated state and the energy balance is used to calculate $\dot{m}_{\text{wf},j}$, that is,

$$\dot{m}_{\text{wf},j} = \frac{D_j}{(h_{\text{j}} - h_{02})} \tag{20}$$

here, h_{02} is the enthalpy of the working fluid entering into the evaporator and h_j is the enthalpy of the saturated fluid at $T_{\text{r},j}$.

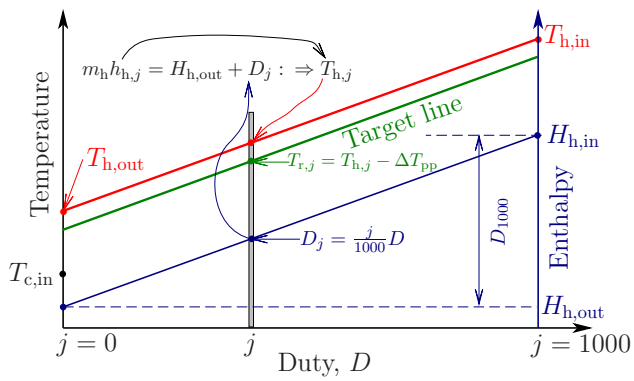

Fig. 3: Graphical demonstration of the target-temperature line construction.

Once the values of $P_{\text{evap},j}$ and $\dot{m}_{\text{wf},j}$ are known, possible state of the fluid leaving the evaporator, state 03, may be estimated using the overall energy balance for the evaporator; that is,

$$h_{03,j} = h_{02} + \frac{D}{\dot{m}_{\text{wf},j}} \tag{21}$$

However, $T_{03,j}$ may hypothetically exceed the target-temperature to satisfy the energy balance equation (Eq. 4), and constitutes the violation of design constraint (ΔT_{pp}) and the second-law of thermodynamics. If $T_{03,j} > (T_{\text{h,in}} - \Delta T_{\text{pp}})$, the solution is non-feasible, and if the fluid is leaving the evaporator in two-phase state with $X_{03} < 0.9$, the solution is also ignored. If $T_{\text{evap,sat},j} > 0.95 T_{\text{cr}}$, the solution is also discarded (Table 1). The procedure is also illustrated in Fig. 4.

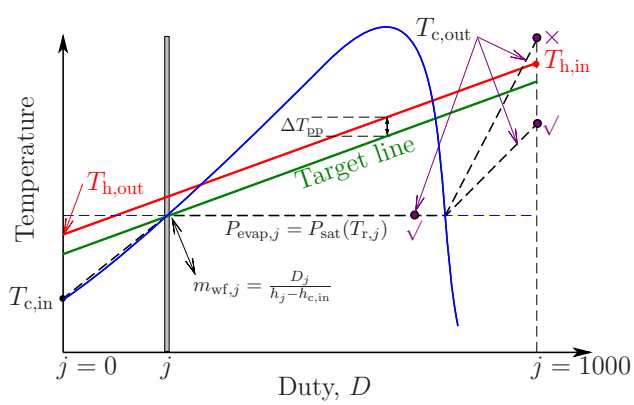

Fig. 4: Illustration of the estimation of the operating parameters.

By considering the pinch point to occur along the length of the heat exchanger, a range of feasible operating parameters (P_{evap}, $T_{evap,sat}$, T_{03} and $\dot{m}_{wf}$) are estimated. Detailed thermodynamic analysis of the cycle is then carried out for all these cases. However, if $X_{04} < 0.9$, the solution is also discarded, and this scenario will not prevail for dry/isentropic fluids. Based on all the feasible solutions, overall exergy efficiency, ε_o, is estimated and the condition that yields the maximum value of ε_o is the optimum operating condition of the working fluid for $T_{h,in}$. At a given $T_{h,in}$, analysis is done for several pre-selected working fluids and the working fluid providing the maximum ε_o is selected as the optimum working fluid and the corresponding operating parameters are chosen for the source temperature.

3 Results and Discussions

Shown in Fig. 5 is an example of the target-temperature line method applied for $T_{h,in}$ = 100°C using R1216 as the working fluid. Using Eq. 17, we get, $D = 40.6$ kW, and D is equally divided into 1000 parts along the length of the heat-exchanger (evaporator) and calculations are done for all the cases. In Fig. 5, only 5 representative cases are presented and some key results are also noted. Hence, cases ② and ③ are feasible solutions, and in-between these there are 179 intermediate feasible solutions. Three other cases of Fig. 5 are non-feasible because of the following reasons:

Case ①: $T_{03} > (T_{h,in} - \Delta T_{pp})$,

Case ④: $T_{evap,sat} > 0.95 T_{cr}$,

Case ⑤: $T_{evap,sat} > 0.95 T_{cr}$, $X_{03} < 0.90$.

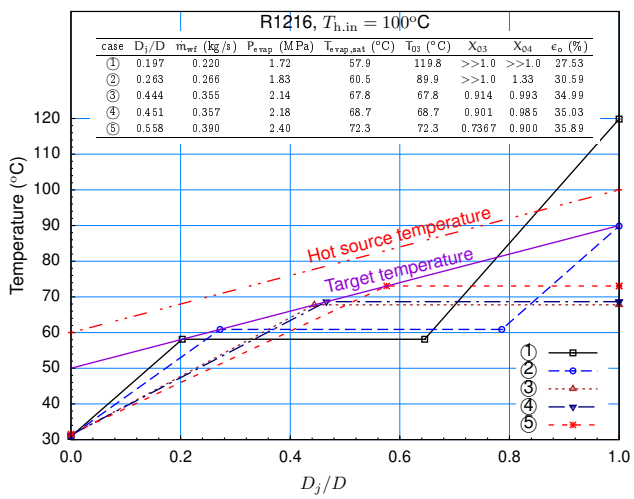

case	D_j/D	$\dot{m}_{wf}$ (kg/s)	P_{evap} (MPa)	$T_{evap,sat}$ (°C)	T_{03} (°C)	X_{03}	X_{04}	ϵ_o (%)
①	0.197	0.220	1.72	57.9	119.8	>>1.0	>>1.0	27.53
②	0.263	0.266	1.83	60.5	89.9	>>1.0	1.33	30.59
③	0.444	0.355	2.14	67.8	67.8	0.914	0.993	34.99
④	0.451	0.357	2.18	68.7	68.7	0.901	0.985	35.03
⑤	0.558	0.390	2.40	72.3	72.3	0.7367	0.900	35.89

Fig. 5: Estimation of the operating parameters for $T_{h,in}$ = 100°C using R1216.

The estimated values of $\dot{m}_{wf}$ and fluid temperatures in the evaporator sections (Fig. 1) versus P_{evap} are plotted in Fig. 6. Hence, lines are drawn to present all the results and symbols are used to show the feasible solutions. It is seen that the feasible solutions are within narrow ranges of evaporator saturation pressure, temperature and mass flow rate. It is also seen that, at low values of $\dot{m}_{wf}$ and P_{evap}, fluid vapour leaves the turbine superheated and the super-heating diminishes with increase in P_{evap}.

Shown in Fig. 7(a) is the energy-flow diagram, for the optimal operating condition for $T_{h,in}$ = 100°C using R1216. Optimum performance is achieved at case ③ of Fig. 5. Hence, only 4.4% of the waste heat is converted to turbine work, the

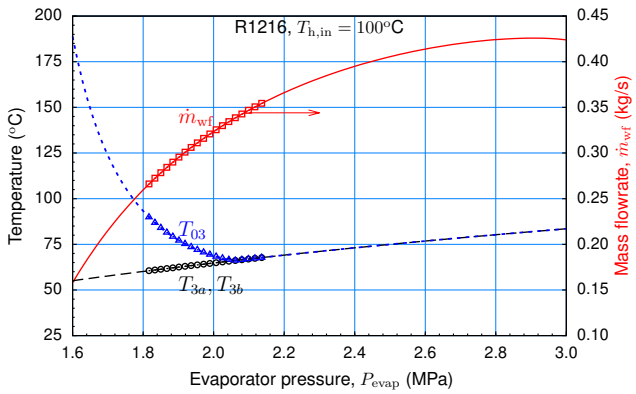

Fig. 6: Variation of $\dot{m}_{wf}$ and temperatures of the working fluid in the evaporator.

pump work is equivalent to 0.7% of heat yielding only 3.8% of the heat to the net output work, and also it seen that pump work is not negligible as compared to turbine work which is common in water-based Rankine cycle. So, overall thermal efficiency is only 3.8%, and 46.6% of the waste heat is exhausted with the hot gases leaving the evaporator at 60°C, and 49.6% heat is rejected to the condenser. However, exergy-flow diagram, shown in Fig. 7(b), depicts significantly different scenario: only 2.8% of the exergy is lost to the condenser, 23.5% is lost with the hot exhaust gases and 35.0% of exergy is converted to net output work. Hence, overall effectiveness of the system is 35.0%. Figure 7(b) shows some details of the exergy consumption: 25.0% is lost due to irreversibility in the evaporator, 11.9% is lost because of turbine irreversibility and 1.8% is lost in the pump. Hence, the evaporator is the component where significant exergy destruction occurs and warrant proper thermal matching between the heat exchanging fluids.

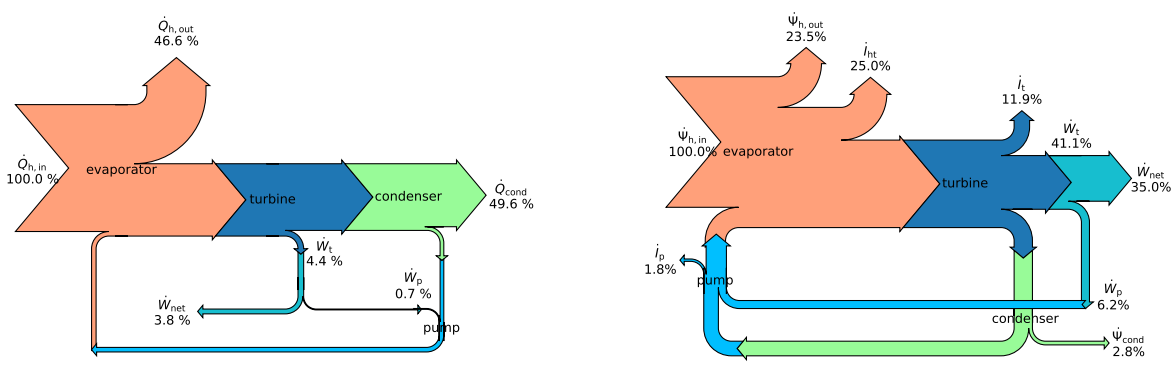

(a) Energy flow.

(b) Exergy flow.

Fig. 7: Energy and Exergy flow in WHR system at optimal condition for $T_{h,in}$ = 100°C using R1216.

Shown in Fig. 8 are the values of $\dot{m}_{wf}$ versus P_{evap} for $T_{h,in}$ = 100°C. Hence, lines are used to represent results for working fluids having critical temperatures lower than $T_{h,in}$ and symbols are used otherwise, and same convention is followed in Figs. 8 to 10. The values of $\dot{m}_{wf}$ increase with increase in P_{evap}. However, these values are widely different between the working fluids as these depend on fluid's liquid-phase specific heat capacity. Shown in Fig. 9 are the values of $\dot{W}_{net}$ versus $T_{evap,sat}$ for $T_{h,in}$ = 100°C. It is seen that the net work increase with increase in $T_{evap,sat}$ for all the fluids, and the maximum output works are reasonably close.

The values of three exergy based performance parameters: ε_{cy}, ε_{ht} and ε_o for several heat source temperatures are plotted in Fig. 10. For a given working fluid, the increase in $T_{evap,sat}$ results in the increase in the evaporator pressure and the inlet pressure of the expander while the expander outlet pressure is fixed by the condensation temperature. Hence, increase in $T_{evap,sat}$ results in the increase of the net output power of the ORC cycle because of the higher expansion ratio in the expander and leads to higher values of ε_{cy}. It is also seen, in Fig. 10, that increase in $T_{h,in}$ results in higher evaporator temperatures and with higher values of ε_{cy}. Hence, the values of ε_{cy} increase with $T_{evap,sat}$ and the maximum values for all the working fluids are found close. In the evaporator, temperature difference between the heat source and the working fluid exists because of the sensible heating of the liquid working fluid is followed by the isothermal evaporation where working fluid temperature deviates further from the hot source temperature. The values of ε_{ht} vary significantly, and therefore affect the overall performance of the system. Hence, effectiveness of the heat exchange process in the evaporator is affected by the mass flow rate of the working fluid and the temperature deviation from the heat source fluid. Larger mass flow rates and larger the temperature difference lead to increase in the exergy destruction in the evaporator [45]. Moreover, working fluid's thermophysical properties like specific heat capacity and the latent heat of evaporation play vital role to determine the mass flow rate and the temperature profile of the working fluid. Although specific heat of the working fluid is not very temperature sensitive, the latent heat of evaporation is reduced with increase in the saturation temperature. At low $T_{evap,sat}$, the temperature of the working fluid leaving the evaporator may be superheated (as can be seen in Fig. 5) with low mass flow rate and therefore may achieve good ε_{ht}. However, with increase in $T_{evap,sat}$, values of the mass flow rate increase with reduction in the evaporator exit temperature and with lower values of ε_{ht}. However, at higher values of $T_{evap,sat}$, mass flow rate is increased and the working fluid gets a significant amount of sensible heating where temperature curve can be close the heat source fluid temperature and isothermal evaporation follows, and results in less deviation from heat source temperature. Therefore, exergy destruction in the evaporator is reduced with increase in the $T_{evap,sat}$. Hence, the values of ε_{ht} initially decrease to a minimum and then increase with increase in $T_{evap,sat}$. It is observed that, one can draw a straight line approximately indicating the values of ε_{ht} once the minima is reached in the plot of ε_{ht} versus $T_{evap,sat}$ (Fig. 10), for all the fluids considered and for all the heat source temperatures. Overall effectiveness of the WHR system is the result of the combined effectiveness of the heat exchange process in the evaporator and the ORC cycle, and their values increase with increase in $T_{evap,sat}$, and increase in $T_{h,in}$ also increase $T_{evap,sat}$ and results in the higher values of ε_o at higher heat source temperatures.

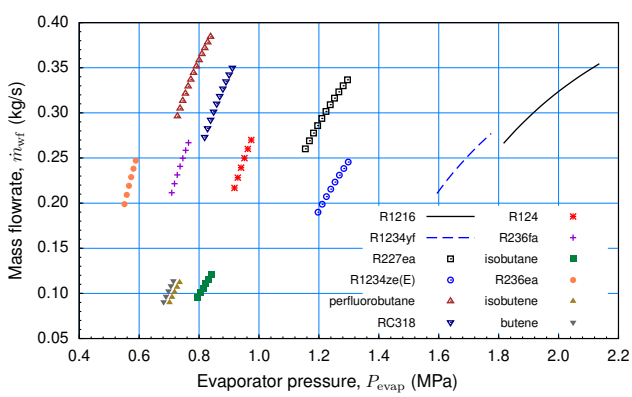

Fig. 8: Variation of $\dot{m}_{wf}$ with P_{evap} for $T_{h,in}$ =100°C.

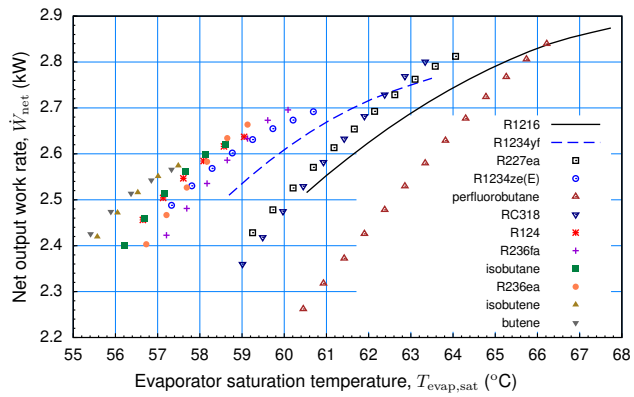

Fig. 9: Variation of $\dot{W}_{net}$ with $T_{evap,sat}$ for $T_{h,in}$ = 100°C.

Key optimal operating and performance parameters obtained from the present study is summarized in Table 5. Hence, the working fluids are arranged in the ascending order of the fluid's critical temperatures, maximum values of the parameters for a given source temperature are underlined and the optimal working fluids are indicated bold-faced. Following observations can also be made:

A. For a given source temperature:

- optimal working fluid's T_{cr} is lower than $T_{h,in}$,
- values of $\dot{m}_{wf}$ and P_{evap} are unrelated to T_{cr},
- values of $T_{evap,sat}$ and T_{03} show some trend to decrease with increase in T_{cr},
- no pattern/relationship is recognised between the performance parameters (ε_{cy}, ε_{ht} and ε_o) and T_{cr}.

B. With increase in source temperatures:

- performance parameters (ε_{cy}, ε_{ht} and ε_o) increase with increase in $T_{h,in}$,
- values of $\dot{m}_{wf}$ and P_{evap} are unrelated to $T_{h,in}$,
- For $T_{h,in} \geq 200$°C, many super-dry working fluids are used and most of these exhibit higher degree of superheat of the vapour leaving the turbine and consequent higher losses to the condenser. These fluids offer lower overall performance with high values of ε_{ht}.
- optimal working fluids are either 'isentropic' or 'dry' type.

Shown in Fig. 11 are the net work output and exergy losses versus $T_{h,in}$ for optimum operating conditions with optimal working fluids. It is noted that, the optimum working fluids are either 'isentropic' or 'dry' type, although many super-dry type working fluids are used for higher source temperatures. In Fig. 11(a), it is seen that, the supply of exergy increase with temperature, net output work also increases with it. Figure 11(a) shows the quantitative data, and Fig. 11(b) shows the percentage-wise results. Clearly, percentage of net output work increases and exergy destructions decrease with increase in source temperature. Overall exergy efficiency is achieved at high source temperature.

In the present study, the correlations between heat source temperature ($T_{h,in}$) and critical properties of optimal working fluid (T_{cr} and P_{cr}), some optimum operating parameters ($T_{evap,sat}$, P_{evap}, P_{cond} and $\dot{m}_{wf}$) and optimum performance parameters (ε_{cy}, ε_{ht} and ε_o) are explored using statistical data analysis. A graphical representation of the estimated correlation coefficient, r (also known as Pearson's r), of the key parameters for the optimal working fluid and the optimum operating conditions

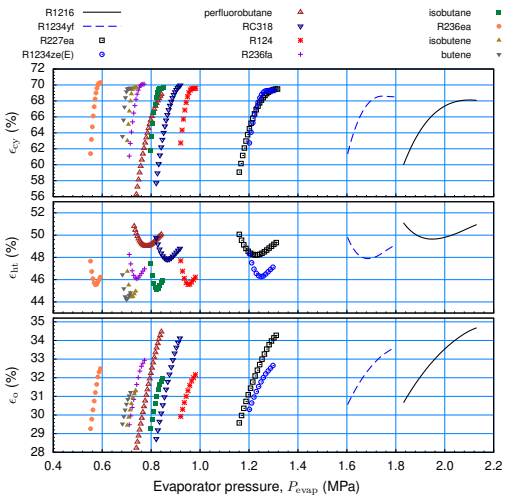

(a) $T_{h,in}$ =100°C.

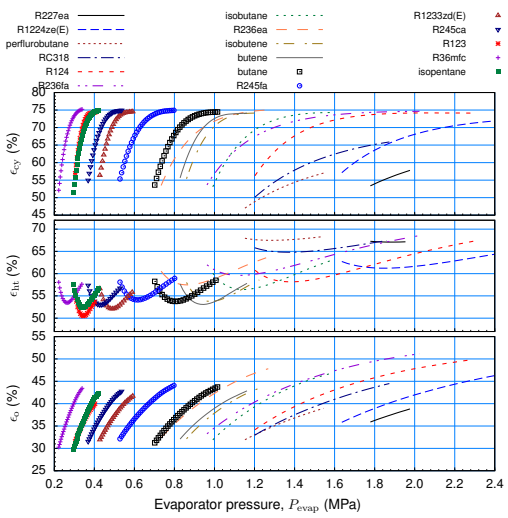

(b) $T_{h,in}$ = 150°C.

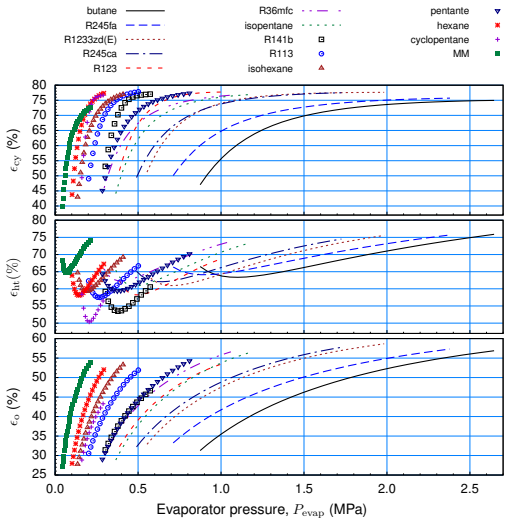

(c) $T_{h,in}$ = 200°C.

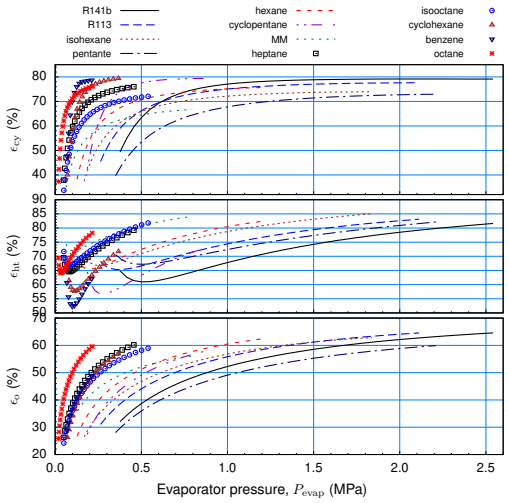

(d) $T_{h,in}$ = 250°C.

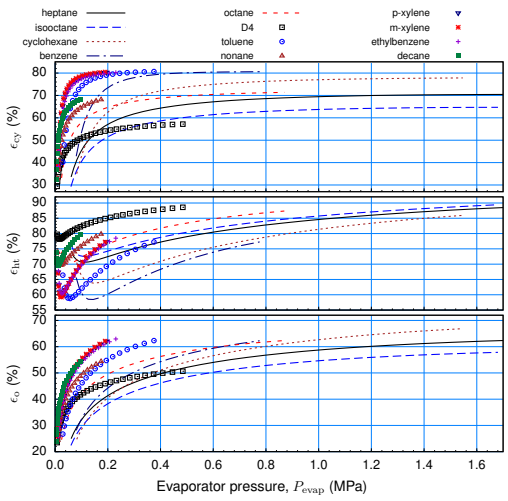

(e) $T_{h,in}$ = 300°C.

Fig. 10: Effects of $T_{evap,sat}$ on ε_{cy}, ε_{ht} and ε_o for $T_{h,in}$ = 100, 150, 200, 250 and 300°C.

Table 5: Optimal operating and performance parameters.

(a) $T_{h,in}$ = 100°C.

working fluid	$\dot{m}_{wf}$ (kg/s)	P_{evap} (MPa)	$T_{evap,sat}$ (°C)	T_{03} (°C)	T_{04} (°C)	ε_{cy} (%)	ε_{ht} (%)	ε_o (%)
R1216	0.355	2.138	67.8	67.8	30	67.9	51.5	35.0
R1234yf	0.28	1.786	63.8	63.8	30	68.4	49.3	33.7
R227ea	0.343	1.309	64.5	64.5	31.8	69.4	49.5	34.4
R1234ze(E)	0.246	1.298	60.7	60.7	30	69.2	47.3	32.7
pefluorobutane	0.385	0.840	66.3	66.3	43.1	68.9	50.2	34.6
RC318	0.355	0.918	63.7	63.7	35.5	70	49	34.3
R124	0.279	0.985	59.5	59.5	30	69.6	46.4	32.3
R236fa	0.272	0.771	60.4	60.4	30	70.1	47	32.9
isobutane	0.123	0.846	58.9	58.9	30	69.6	46	32.0
R236ea	0.254	0.594	59.5	59.5	30	70.3	46.4	32.6
isobutene	0.114	0.739	57.7	57.7	30	69.6	45.1	31.4
butene	0.114	0.715	57.4	57.4	30	69.6	44.9	31.2

(b) $T_{h,in}$ = 125°C.

working fluid	$\dot{m}_{wf}$ (kg/s)	P_{evap} (MPa)	$T_{evap,sat}$ (°C)	T_{03} (°C)	T_{04} (°C)	ε_{cy} (%)	ε_{ht} (%)	ε_o (%)
R1234yf	0.376	2.332	76.3	87.6	47.9	69.8	59.2	41.3
R227ea	0.486	1.980	82.9	85.0	46.1	70.8	61.6	43.6
R1234ze(E)	0.384	1.814	75.3	75.3	30.0	71.8	57.7	41.4
perfluorobutane	0.550	1.398	88.7	88.7	55.2	69.2	63.1	43.6
RC318	0.526	1.417	82.4	82.4	44.2	71.9	60.9	43.8
R124	0.436	1.289	70.9	70.9	30.0	72.1	54.9	39.6
R236fa	0.421	1.062	73.2	73.2	31.1	72.7	56.2	40.9
isobutane	0.192	1.063	69.0	69.0	30.0	72.1	53.6	38.6
R236ea	0.394	0.791	70.4	70.4	30.7	72.9	54.4	39.7
isobutene	0.181	0.898	66.0	66.0	30.0	72.0	51.4	37.0
butene	0.181	0.860	65.2	65.2	30.0	71.9	50.8	36.5
butane	0.177	0.739	66.1	66.1	30.0	72.2	51.5	37.2
R245fa	0.334	0.553	66.4	66.4	30.0	72.6	51.7	37.5
R1233zd(E)	0.339	0.440	64.3	64.3	30.0	72.4	50.1	36.3
R245ca	0.311	0.383	65.3	65.3	30.0	72.7	50.8	37.0

(c) $T_{h,in}$ = 150°C.

working fluid	$\dot{m}_{wf}$ (kg/s)	P_{evap} (MPa)	$T_{evap,sat}$ (°C)	T_{03} (°C)	T_{04} (°C)	ε_{cy} (%)	ε_{ht} (%)	ε_o (%)
R227ea	0.486	1.981	83.0	129.8	98.4	58.6	67.1	39.3
R1234ze(E)	0.442	2.484	90.2	103.7	51.9	72.5	65.4	47.4
perfluorobutane	0.567	1.559	93.9	123.5	95.8	57.6	68.6	39.5
RC318	0.577	1.881	95.7	113.5	77.3	66.3	67.9	45.0
R124	0.570	2.214	96.4	96.4	30.0	74.1	67.2	49.8
R236fa	0.538	1.971	100.9	100.9	38.7	74.6	68.7	51.2
isobutane	0.250	1.565	87.6	87.6	32.5	74.2	63.0	46.8
R236ea	0.509	1.251	89.5	89.5	38.3	75.0	63.7	47.8
isobutene	0.240	1.222	79.9	79.9	30.0	74.2	58.7	43.6
butene	0.242	1.149	78.2	78.2	30.0	74.0	57.7	42.7
butane	0.233	1.005	79.7	79.7	30.0	74.4	58.6	43.6
R245fa	0.440	0.796	80.3	80.3	30.0	74.9	58.9	44.1
R1233zd(E)	0.452	0.591	75.7	75.7	30.0	74.5	56.0	41.7
R245ca	0.412	0.534	77.5	77.5	30.0	74.9	57.1	42.7
R123	0.511	0.402	72.4	72.4	30.0	74.3	53.7	39.9
R365mfc	0.415	0.337	78.4	78.4	35.8	75.2	57.7	43.4
isopentane	0.239	0.420	76.6	76.6	32.7	74.8	56.6	42.3

(d) $T_{h,in}$ = 175°C.

working fluid	$\dot{m}_{wf}$ (kg/s)	P_{evap} (MPa)	$T_{evap,sat}$ (°C)	T_{03} (°C)	T_{04} (°C)	ε_{cy} (%)	ε_{ht} (%)	ε_o (%)
isobutane	0.275	2.568	114.3	119.3	54.5	74.5	73.1	54.4
R236ea	0.566	2.306	118.6	121.4	58.1	74.8	73.8	55.2
isobutene	0.285	2.147	108.5	108.5	32.3	75.8	70.5	53.5
butene	0.289	1.911	103.6	103.6	30.0	75.8	68.5	51.9
butane	0.275	1.674	104.8	104.8	38.1	76.1	68.9	52.5
R245fa	0.521	1.424	105.4	105.4	37.8	76.7	68.9	52.8
R1233zd(E)	0.546	0.917	94.2	94.2	30.4	76.4	64.0	48.9
R245ca	0.493	0.863	96.8	96.8	37.7	76.8	65.1	49.9
R123	0.623	0.584	87.2	87.2	30.0	76.2	60.3	45.9
R365mfc	0.491	0.557	97.8	97.8	45.8	76.7	65.5	50.2
isopentane	0.284	0.645	94.8	94.8	42.3	76.5	64.3	49.2
R141b	0.496	0.402	78.1	78.1	30.0	75.5	54.8	41.4
R113	0.686	0.308	85.8	85.8	32.8	76.4	59.4	45.4
isohexane	0.282	0.243	90.7	90.7	43.0	76.6	62.1	47.6

(e) $T_{h,in}$ = 200°C.

working fluid	$\dot{m}_{wf}$ (kg/s)	P_{evap} (MPa)	$T_{evap,sat}$ (°C)	T_{03} (°C)	T_{04} (°C)	ε_{cy} (%)	ε_{ht} (%)	ε_o (%)
butane	0.286	2.665	130.7	139.6	65.8	75.2	76.7	57.6
R245fa	0.546	2.464	132.5	141.1	65.0	75.9	76.7	58.3
R1244zd(E)	0.633	2.278	134.0	140.7	63.4	76.0	76.5	58.1
R245ca	0.546	1.735	129.3	129.3	51.2	77.6	75.0	58.1
R123	0.710	0.995	110.9	110.9	35.0	77.7	68.9	53.5
R365mfc	0.538	1.072	126.9	126.9	61.1	76.8	74.2	57.0
isopentane	0.311	1.163	123.5	123.5	57.3	77.0	73.5	56.6
R141b	0.578	0.592	94.1	94.1	30.0	77.1	61.3	47.3
R113	0.779	0.500	105.9	105.9	42.5	77.8	66.7	51.9
Isohexane	0.313	0.423	113.3	113.3	56.9	77.2	69.8	53.9
pentane	0.305	0.834	115.8	115.8	51.5	77.5	70.8	54.9
hexane	0.307	0.306	108.7	108.7	51.9	77.6	68.0	52.8
cyclopentane	0.329	0.292	85.6	85.6	30.0	76.7	56.7	43.5
MM	0.396	0.214	128.6	128.6	82.9	72.8	74.4	54.1

(f) $T_{h,in}$ = 225°C.

working fluid	$\dot{m}_{wf}$ (kg/s)	P_{evap} (MPa)	$T_{evap,sat}$ (°C)	T_{03} (°C)	T_{04} (°C)	ε_{cy} (%)	ε_{ht} (%)	ε_o (%)
R123	0.755	2.524	160.8	160.8	49.3	78.3	81.5	63.8
R365mfc	0.551	2.180	163.8	165.4	86.7	74.6	81.9	61.1
isopentane	0.316	2.356	164.1	165.0	83.5	75.0	82.6	61.9
R141b	0.639	1.014	119.1	119.1	30.0	78.4	69.8	54.7
R113	0.841	0.914	134.6	134.6	55.9	78.3	74.6	58.5
isohexane	0.329	0.813	144.5	144.5	76.1	76.4	77.6	59.3
pentane	0.318	1.782	156.5	156.5	71.4	76.9	80.6	62.0
hexane	0.325	0.581	137.1	137.1	69.4	77.3	75.5	58.4
cyclopentane	0.367	0.465	104.7	104.7	30.0	78.2	64.0	50.1
MM	0.411	0.420	158.5	158.5	104.5	70.2	79.9	56.1
heptane	0.329	0.240	130.8	130.8	68.4	77.5	73.6	57.0
isooctane	0.350	0.289	141.0	141.0	85.2	74.7	76.6	57.2

(g) $T_{h,in}$ = 250°C.

working fluid	$\dot{m}_{wf}$ (kg/s)	P_{evap} (MPa)	$T_{evap,sat}$ (°C)	T_{03} (°C)	T_{04} (°C)	ε_{cy} (%)	ε_{ht} (%)	ε_o (%)
R141b	0.670	2.429	168.0	168.0	43.0	79.1	81.7	64.6
R113	0.867	2.112	182.6	182.6	74.9	77.7	83.7	65.1
isohexane	0.329	1.812	190.4	190.4	102.2	74.0	85.4	63.2
pentane	0.316	2.335	173.0	187.4	104.8	73.2	83.3	61.0
hexane	0.331	1.183	174.5	174.5	92.2	75.7	82.5	62.5
cyclopentane	0.389	0.861	133.7	133.7	37.7	79.4	72.9	57.9
MM	0.416	0.820	193.4	193.4	129.1	66.9	84.5	56.6
heptane	0.339	0.480	162.0	162.0	89.0	76.2	79.8	60.8
isooctane	0.356	0.555	173.0	173.0	108.4	72.2	82.1	59.3
cyclohexane	0.385	0.390	133.3	133.3	51.0	79.5	72.6	57.8
benzene	0.405	0.224	108.3	108.3	30.0	78.8	63.1	49.7
octane	0.343	0.223	156.7	156.7	88.3	76.3	78.6	60.0

(h) $T_{h,in}$ = 275°C.

working fluid	$\dot{m}_{wf}$ (kg/s)	P_{evap} (MPa)	$T_{evap,sat}$ (°C)	T_{03} (°C)	T_{04} (°C)	ε_{cy} (%)	ε_{ht} (%)	ε_o (%)
pentane	0.316	2.335	173.0	215.4	137.7	68.3	83.4	57.0
hexane	0.327	2.082	209.2	213.7	123.2	72.2	87.3	63.0
cyclopentane	0.393	1.919	179.0	179.0	60.8	79.8	82.8	66.0
MM	0.414	1.278	219.6	225.8	157.9	62.5	87.3	54.6
heptane	0.341	0.965	199.1	199.1	113.6	74.0	85.1	63.0
isooctane	0.354	1.059	210.0	210.0	135.1	68.9	86.8	59.8
cyclohexane	0.392	0.769	167.2	167.2	72.5	79.4	79.9	63.4
benzene	0.430	0.410	133.6	133.6	30.0	79.9	70.5	56.3
octane	0.346	0.452	189.7	189.7	111.6	74.2	83.6	62.0
D4	0.488	0.261	217.3	217.3	161.6	60.7	86.2	52.3
toluene	0.434	0.194	135.1	135.1	36.0	80.0	71.0	56.8
nonane	0.349	0.176	173.0	173.2	113.5	73.4	80.6	59.1

(i) $T_{h,in}$ = 300°C.

working fluid	$\dot{m}_{wf}$ (kg/s)	P_{evap} (MPa)	$T_{evap,sat}$ (°C)	T_{03} (°C)	T_{04} (°C)	ε_{cy} (%)	ε_{ht} (%)	ε_o (%)
heptane	0.335	1.850	239.9	240.5	144.0	70.5	89.5	63.1
isooctane	0.347	1.757	243.5	246.2	165.6	64.8	90.1	58.4
cyclohexane	0.388	1.581	210.4	210.4	100.4	77.9	86.5	67.4
benzene	0.442	0.823	167.8	167.8	40.2	80.6	78.1	63.0
octane	0.344	0.898	227.6	227.6	138.1	71.5	87.8	62.7
D4	0.487	0.485	249.9	249.9	187.9	57.2	88.7	50.7
toluene	0.445	0.394	166.6	166.6	54.2	80.7	77.9	62.9
nonane	0.349	0.176	173.0	204.4	144.6	68.2	79.9	54.5
p-Xylene	0.443	0.213	168.5	168.5	64.5	80.5	78.2	63.0
m-Xylene	0.443	0.199	166.1	166.1	62.8	80.5	77.7	62.6
ethylbenze	0.436	0.244	172.3	172.3	69.4	80.3	79.1	63.5
decane	0.351	0.106	175.9	202.0	142.6	68.7	80.3	55.2

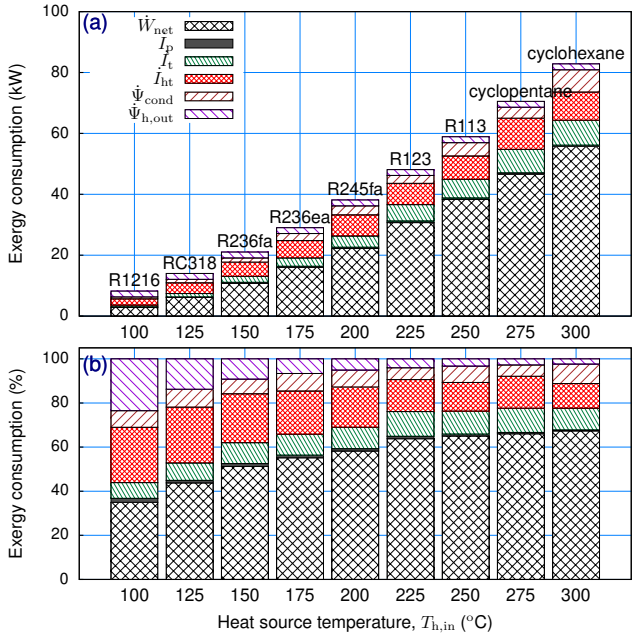

Fig. 11: Work output and exergy destruction for $T_{h,in}$ = 100° to 300°C for optimal working fluid with optimal operating conditions: (a) quantitative results, (b) percentage-wise results.

are displayed in the form of a heat-map in Fig. 12. Hence, the value of r is a measure of the extent to which the variables are linearly related and the value lies between +1 and -1: a value near +1 indicates a strong positive linear relationship, whereas a value close to -1 suggests a strong negative linear relationship, and a value close to 0 does not rule out any strong relationship – there could still be a strong relationship but one that is not linear [46]. It is seen in Fig. 12 that the values of T_{cr}, P_{cr}, $T_{evap,sat}$, P_{cond}, ε_{cy}, ε_{ht} and ε_o have very strong correlations with $T_{h,in}$, and the values of P_{cond} exhibit strong correlations to the effectiveness. However, working fluid is saturated at 30°C leaving the condenser and therefore the value of P_{cond} is fixed once the working fluid is selected. It may also be noted that, P_{evap} is not an independent parameter, once $T_{evap,sat}$ is set, its value is also fixed. Therefore, correlations are obtained for T_{cr}, P_{cr}, $T_{evap,sat}$, ε_{cy}, ε_{ht} and ε_o as function of $T_{h,in}$ for the optimal working fluid and optimum operating conditions.

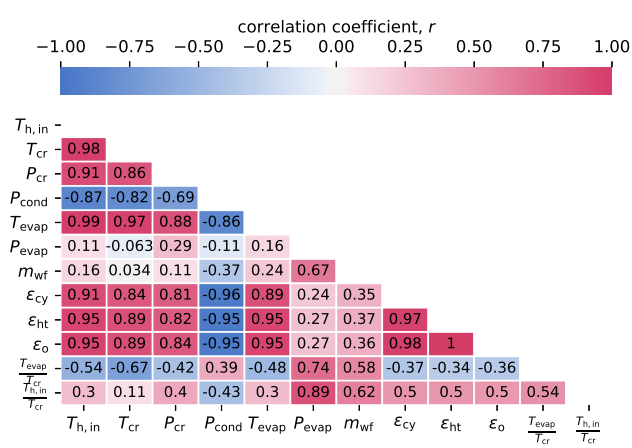

Fig. 12: Heat-map of the key optimal parameters of WHR system for $T_{h,in}$ = 100°C to 300°C.

Shown in Fig. 13 are the variations of the optimum $T_{\text{evap,sat}}$, T_{cr} and P_{cr} plotted as function of $T_{\text{h,in}}$. Values of $T_{\text{evap,sat}}$, T_{cr} and P_{cr} are found to increase with increase in $T_{\text{h,in}}$. As can be seen in Fig. 13, linear fits represent the data well and the estimated values of r's are 0.992, 0.982 and 0.907 for T_{evap}, T_{cr} and P_{cr}, respectively. The correlations with $T_{\text{h,in}}$ can be expressed as:

$$T_{\text{evap,sat}}\ (^{\text{o}}\text{C}) = -4.728 + 0.7107\ T_{\text{h,in}}\ (^{\text{o}}\text{C}) \tag{22}$$

$$T_{\text{cr}}\ (^{\text{o}}\text{C}) = -10.71 + 0.9014\ T_{\text{h,in}}\ (^{\text{o}}\text{C}) \tag{23}$$

$$P_{\text{cr}}\ (\text{MPa}) = 2.116 + 0.007604\ T_{\text{h,in}}\ (^{\text{o}}\text{C}) \tag{24}$$

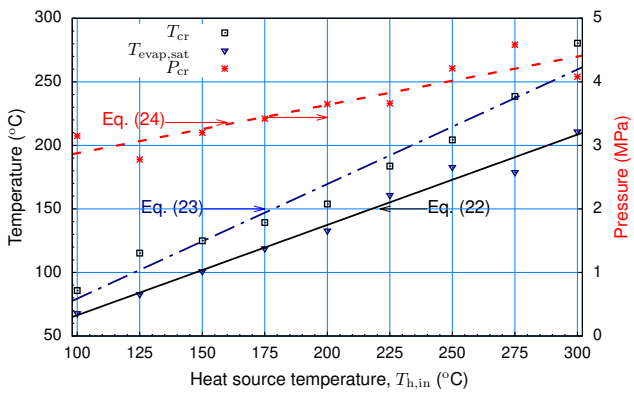

Fig. 13: Variation of optimum $T_{\text{evap,sat}}$ and critical properties of the optimal working fluid for different $T_{\text{h,in}}$.

Shown in Fig. 14 are the variations of ε_{cy}, ε_{ht} and ε_{o} with $T_{\text{h,in}}$ for optimal operating conditions with optimal working fluid. All the effectiveness values increase with increase in $T_{\text{h,in}}$. It is seen that the values of ε_{cy} are less sensitive to the variations of $T_{\text{h,in}}$, while the values of ε_{ht} sharply increase with an increase in $T_{\text{h,in}}$, and results in a moderate increase of the values of ε_{o} with increase in $T_{\text{h,in}}$. As can be seen in Fig. 14, linear fits describe the data well and the estimated values of r's are 0.907, 0.949 and 0.953 for ε_{cy}, ε_{ht} and ε_{o}, respectively. The correlations with $T_{\text{h,in}}$ can be expressed as:

$$\varepsilon_{\text{cy}}\ (\%) = 65.64 + 0.04893\ T_{\text{h,in}}\ (^{\text{o}}\text{C}) \tag{25}$$

$$\varepsilon_{\text{ht}}\ (\%) = 41.56 + 0.1623\ T_{\text{h,in}}\ (^{\text{o}}\text{C}) \tag{26}$$

$$\varepsilon_{\text{o}}\ (\%) = 25.17 + 0.1551\ T_{\text{h,in}}\ (^{\text{o}}\text{C}) \tag{27}$$

4 Conclusions

In the present study, a simple target-temperature-line approach is proposed and used to get the optimum operating parameters and suitable working fluids for the sub-critical ORC based WHR system. It is seen that the optimal fluids have critical temperatures lower than the heat source temperatures and the optimal fluids are either 'isentropic' or 'dry' type fluid. At a given heat source temperature, no other pattern is recognized indicating the relationship between optimal working fluid's critical properties (T_{cr} and P_{cr}), evaporator saturation temperature ($T_{\text{evap,sat}}$) and performance indicators (ε_{cy}, ε_{ht} and ε_{o}). However, some optimal parameters (T_{cr}, P_{cr} and $T_{\text{evap,sat}}$) and performance indicators (ε_{cy}, ε_{ht} and ε_{o}) are found linearly correlated with the heat source temperature, and excellent correlating equations are established. These correlations offer guidance for the pre-selection of the working fluids and predictions of the operating/performance parameters. Hence, using the proposed target-temperature line approach and analysis with enough suitable working fluids could lead to the optimum utilization of waste heat.

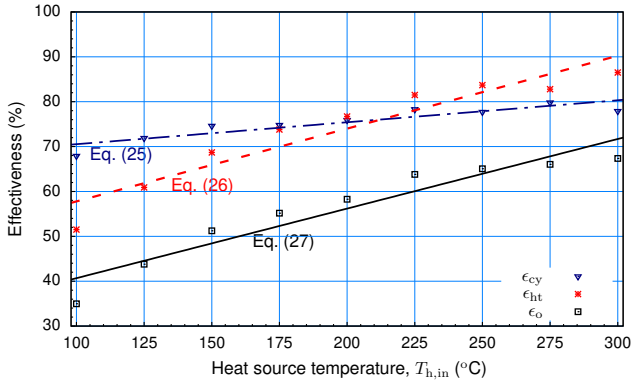

Fig. 14: Effects of $T_{h,in}$ on ε_{cy}, ε_{ht} and ε_o for optimum operating conditions with optimal working fluid.

Acknowledgements

The project is carried out at Bangladesh University of Engineering and Technology (BUET), Dhaka-1000, Bangladesh.

References

[1] Woodland, B. J., Ziviani, D., Braun, J. E., and Groll, E. A., 2020. "Considerations on alternative organic rankine cycle congurations for low-grade waste heat recovery". *Energy,* **193**, p. 116810.

[2] Bendig, M., Maréchal, F., and Favrat, D., 2013. "Defining "waste heat" for industrial processes". *Applied Thermal Engineering,* **61**, pp. 134 – 142.

[3] Dumont, O., Dickes, R., Rosa, M. D., Douglas, R., and Lemort, V., 2018. "Technical and economic optimization of subcritical, wet expansion and transcritical organic rankine cycle (orc) systems coupled with a biogas power plant". *Energy Conversion and Management,* **157**, pp. 294 – 306.

[4] Li, J., Ge, Z., Duan, Y., and Yang, Z., 2019. "Design and performance analyses for a novel organic rankine cycle with supercritical-subcritical heat absorption process coupling". *Applied Energy,* **235**, pp. 1400 – 1414.

[5] Chen, H., Goswami, D. Y., and Stefanakos, E. K., 2010. "A review of thermodynamic cycles and working fluids for the conversion of low-grade heat". *Renewable and Sustainable Energy Reviews,* **14**, pp. 3059 – 3067.

[6] Kim, Y. M., Shin, D. G., Kim, C. G., and Cho, G. B., 2016. "Single-loop organic rankine cycles for engine waste heat recovery using both low- and high-temperature heat sources". *Energy,* **96**, pp. 482 – 494.

[7] Yang, F., Dong, X., Zhang, H., Wang, Z., Yang, K., Zhang, J., Wang, E., Liu, H., and Zhao, G., 2014. "Performance analysis of waste heat recovery with a dual loop organic rankine cycle (ORC) system for diesel engine under various operating conditions". *Energy Conversion and Management,* **80**, pp. 243–255.

[8] Shu, G., Wang, X., and Tian, H., 2016. "Theoretical analysis and comparison of rankine cycle and different organic rankine cycles as waste heat recovery system for a large gaseous fuel internal combustion engine". *Applied Thermal Engineering,* **108**, pp. 525 – 537.

[9] Ahmed, A., Esmaeil, K. K., Irfan, M. A., and Al-Mufadi, F. A., 2018. "Design methodology of organic rankine cycle for waste heat recovery in cement plants". *Applied Thermal Engineering,* **129**, pp. 421 – 430.

[10] Önder Kaşka, 2014. "Energy and exergy analysis of an organic rankine for power generation from waste heat recovery in steel industry". *Energy Conversion and Management,* **77**, pp. 108 – 117.

[11] Mirzaei, M., Ahmadi, M. H., Mobin, M., Nazari, M. A., and Alayi, R., 2018. "Energy, exergy and economics analysis of

an orc working with several fluids and utilizes smelting furnace gases as heat source". *Thermal Science and Engineering Progress,* **5**, pp. 230 – 237.

[12] Liao, G., E, J., Zhang, F., Chen, J., and Leng, E., 2020. "Advanced exergy analysis for organic rankine cycle-based layout to recover waste heat of flue gas". *Applied Energy,* **266**, p. 114891.

[13] Walraven, D., Laenen, B., and D'haeseleer, W., 2013. "Comparison of thermodynamic cycles for power production from low-temperature geothermal heat sources". *Energy Conversion and Management,* **66**, pp. 220 – 233.

[14] Yamankaradeniz, N., Bademlioglu, A., and Kaynakli, O., 2018. "Performance assessments of organic rankine cycle with internal heat exchanger based on exergetic approach". *Journal of Energy Resources Technology,* **140**, p. 102001.

[15] Yang, J., Li, J., Yang, Z., and Duan, Y., 2019. "Thermodynamic analysis and optimization of a solar organic rankine cycle operating with stable output". *Energy Conversion and Management,* **187**, pp. 459–471.

[16] Drescher, U., and Brüggemann, D., 2007. "Fluid selection for the organic rankine cycle (ORC) in biomass power and heat plants". *Applied Thermal Engineering,* **27**, pp. 223–228.

[17] Dai, B., Zhu, K., Wang, Y., Sun, Z., and Liu, Z., 2019. "Evaluation of organic rankine cycle by using hydrocarbons as working fluids: Advanced exergy and advanced exergoeconomic analyses". *Energy Conversion and Management,* **197**, p. 111876.

[18] Zhao, Y., Liu, G., Li, L., Yang, Q., Tang, B., and Liu, Y., 2019. "Expansion devices for organic rankine cycle (ORC) using in low temperature heat recovery: A review". *Energy Conversion and Management,* **199**, p. 111944.

[19] Holik, M., Živić, M., Virag, Z., and Barac, A., 2019. "Optimization of an organic rankine cycle constrained by the application of compact heat exchangers". *Energy Conversion and Management,* **188**, pp. 333 – 345.

[20] Xu, W., Zhao, L., Mao, S. S., and Deng, S., 2020. "Towards novel low temperature thermodynamic cycle: A critical review originated from organic rankine cycle". *Applied Energy,* **270**, p. 115186.

[21] Wu, S.-Y., Zhou, S.-M., Xiao, L., Li, Y.-R., Liu, C., and Xu, J.-L., 2014. "Determining the optimal pinch point temperature difference of evaporator for waste heat recovery". *Journal of the Energy Institute,* **87**, pp. 140–151.

[22] Liu, B.-T., Chien, K.-H., and Wang, C.-C., 2004. "Effect of working fluids on organic rankine cycle for waste heat recovery". *Energy,* **29**, pp. 1207 – 1217.

[23] Zhang, X., Zhang, Y., and Wang, J., 2020. "New classification of dry and isentropic working fluids and a method used to determine their optimal or worst condensation temperature used in organic rankine cycle". *Energy,* **201**, p. 117722.

[24] Chen, G., An, Q., Wang, Y., Zhao, J., Chang, N., and Alvi, J., 2019. "Performance prediction and working fluids selection for organic rankine cycle under reduced temperature". *Applied Thermal Engineering,* **153**, pp. 95 – 103.

[25] Sarkar, J., 2018. "Generalized pinch point design method of subcritical-supercritical organic rankine cycle for maximum heat recovery". *Energy,* **143**, pp. 141 – 150.

[26] Zhu, S., Deng, K., and Qu, S., 2013. "Energy and exergy analyses of a bottoming rankine cycle for engine exhaust heat recovery". *Energy,* **58**, pp. 448 – 457.

[27] Sun, J., Liu, Q., and Duan, Y., 2018. "Effects of evaporator pinch point temperature difference on thermo-economic performance of geothermal organic rankine cycle systems". *Geothermics,* **75**, pp. 249 – 258.

[28] Jankowski, M., Borsukiewicz, A., Szopik-Depczyńska, K., and Ioppolo, G., 2019. "Determination of an optimal pinch point temperature difference interval in ORC power plant using multi-objective approach". *Journal of Cleaner Production,* **217**, pp. 798–807.

[29] Rad, E. A., Mohammadi, S., and Tayyeban, E., 2020. "Simultaneous optimization of working fluid and boiler pressure

in an organic rankine cycle for different heat source temperatures". *Energy,* **194**, p. 116856.

[30] Arriola-Medellín, A., Manzanares-Papayanopoulos, E., and Romo-Millares, C., 2014. "Diagnosis and redesign of power plants using combined pinch and exergy analysis". *Energy,* **72**, pp. 643–651.

[31] Hamsani, M. N., Walmsley, T. G., Liew, P. Y., and Alwi, S. R. W., 2018. "Combined pinch and exergy numerical analysis for low temperature heat exchanger network". *Energy,* **153**, pp. 100–112.

[32] Sarkar, J., 2018. "A Novel Pinch Point Design Methodology Based Energy and Economic Analyses of Organic Rankine Cycle". *Journal of Energy Resources Technology,* **140**, pp. 052004–1 –8.

[33] Yu, H., Feng, X., and Wang, Y., 2015. "A new pinch based method for simultaneous selection of working fluid and operating conditions in an ORC (organic rankine cycle) recovering waste heat". *Energy,* **90**, pp. 36–46.

[34] Lampe, M., Stavrou, M., Bücker, H. M., Gross, J., and Bardow, A., 2014. "Simultaneous Optimization of Working Fluid and Process for Organic Rankine Cycles Using PC-SAFT". *Industrial & Engineering Chemistry Research,* **53**, pp. 8821–8830.

[35] Park, B.-S., Usman, M., Imran, M., and Pesyridis, A., 2018. "Review of organic rankine cycle experimental data trends". *Energy Conversion and Management,* **173**, oct, pp. 679–691.

[36] Feng, Y., Wang, X., Niaz, H., Hung, T.-C., xia He, Z., Jahan Zeb, A., and Xi, H., 2020. "Experimental comparison of the performance of basic and regenerative organic rankine cycles". *Energy Conversion and Management,* **223**, p. 113459.

[37] Hærvig, J., Sørensen, K., and Condra, T., 2016. "Guidelines for optimal selection of working fluid for an organic rankine cycle in relation to waste heat recovery". *Energy,* **96**, pp. 592–602.

[38] Moran, M., 1989. *Availability Analysis: A Guide to Efficient Energy Use*. ASME Press.

[39] Wark, K., 1995. *Advanced Thermodynamics for Engineers*. McGraw-Hill.

[40] Ayres, R. U., Peiró, L. T., and Méndez, G. V., 2011. "Exergy efficiency in industry: Where do we stand?". *Environmental Science & Technology,* **45**, pp. 10634–10641.

[41] Morosuk, T., and Tsatsaronis, G., 2019. "Splitting physical exergy: Theory and application". *Energy,* **167**, pp. 698–707.

[42] Lemmon, E. W., , Bell, I. H., Huber, M. L., and McLinden, M. O., 2018. NIST Standard Reference Database 23: Reference Fluid Thermodynamic and Transport Properties-REFPROP, Version 10.0, National Institute of Standards and Technology.

[43] Bell, I. H., Wronski, J., Quoilin, S., and Lemort, V., 2014. "Pure and pseudo-pure fluid thermophysical property evaluation and the open-source thermophysical property library coolprop". *Industrial & Engineering Chemistry Research,* **53**(6), pp. 2498–2508.

[44] Nellis, G., and Klein, S., 2009. *Heat Transfer*. Cambridge University Press.

[45] Zhai, H., An, Q., and Shi, L., 2016. "Analysis of the quantitative correlation between the heat source temperature and the critical temperature of the optimal pure working fluid for subcritical organic rankine cycles". *Applied Thermal Engineering,* **99**, pp. 383 – 391.

[46] Peck, R., Olsen, C., and Devore, J., 2016. *Introduction to Statistics and Data Analysis*, 5 ed. Cengage Learning.